## S1 FAGE calibration for $HO_2$ at atmospheric pressure using $H_2O$ vapour photolysis

Figure S1 shows an example of FAGE calibration plot obtained by using the photolysis of water at 185 nm in air to generate known concentrations $HO_2$. The average calibration constant was:

$C_{HO2} = (2.6 \pm 0.4) \times 10^{-7}$ counts $cm^3$ $molecule^{-1}$ $s^{-1}$ $mW^{-1}$,

where the error is a combination of systematic and statistical uncertainties at the $1\sigma$ level.

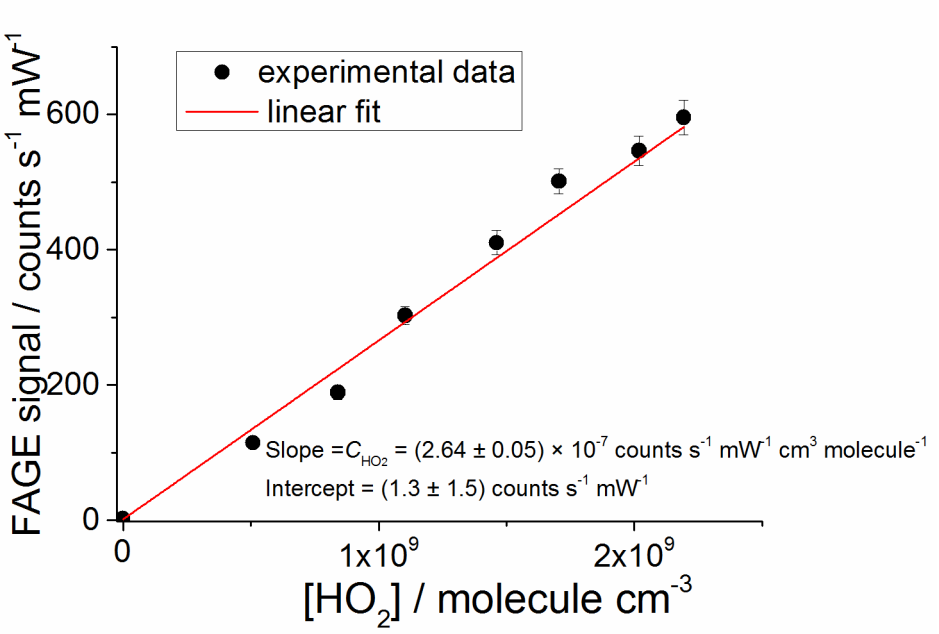


**Figure S1**. FAGE calibration for $HO_2$ at atmospheric pressure and 293 K; laser power = (3.7 ± 0.1) mW; pressure in the detection cell = (3.24 ± 0.20) mbar. The FAGE signal, including the measurement with the Hg lamp turned off ($[HO_2] = 0$), was obtained by subtraction of the online signal in the absence of NO from the signal in the presence of NO (~ $6 \times 10^{13}$ molecule $cm^{-3}$). Averaging time per point = 120 s. The error limits in [HO2] and the FAGE signal are representative for the $1\sigma$ statistical uncertainty.

## S2 Kinetics of the FAGE $HO_2$ signal temporal decay at 1000 mbar

The kinetics of the temporal decay of the fluorescence $HO_2$ signal at 1000 mbar monitored by FAGE when HIRAC UV lamps were extinguished has been used to determine the FAGE calibration factor, $C_{HO2}$, in order to compare it with $C_{HO2}$ obtained by using the water photolysis method (Sect. S1). Eight determinations (Table S1) have been carried out using Eq. (S1) (Eq. (4) in the main text):

$$(S_{HO_2})_t = \left( \left( \frac{1}{(S_{HO_2})_0} + \frac{2 \cdot k_{self\text{-}r.}}{k_{loss} \cdot C_{HO_2}} \right) \times \exp(k_{loss} t) - \left( \frac{2 \cdot k_{self\text{-}r.}}{k_{loss} \cdot C_{HO_2}} \right) \right)^{-1}, \qquad \text{(S1)}$$

where $(S_{HO2})_t$ is the fluorescence signal at reaction time $t$, $(S_{HO2})_0$ is the signal at time $t = 0$, when the lamps were turned off, $k_{self\text{-}r.}$ is the overall $HO_2$ self-reaction rate coefficient, i.e. the sum of the bimolecular rate coefficient of Reaction (R1) and the termolecular rate coefficient of Reaction (R2) at 1000 mbar of air, and $k_{loss}$ is the rate coefficient describing the $HO_2$ wall-loss.

$$HO_2 + HO_2 \rightarrow H_2O_2 + O_2 \quad \text{(R1)}$$

$$HO_2 + HO_2 + M \rightarrow H_2O_2 + O_2 + M \qquad (M = N_2 \text{ or } O_2) \quad \text{(R2)}$$

$$HO_2 \rightarrow \text{loss} \quad \text{(R3)}$$

The average value of the eight independent determinations was:

$C_{HO2} = (2.4 \pm 0.5) \times 10^{-7}$ counts $cm^3$ $molecule^{-1}$ $s^{-1}$ $mW^{-1}$,

where the error is the overall uncertainty obtained by combining the systematic and statistical uncertainties at the $1\sigma$ level.

**Table S1**. FAGE calibration factor for $HO_2$, $C_{HO2}$, and the rate coefficient of the $HO_2$ wall-loss within HIRAC, $k_{loss}$, at 1000 mbar extracted by fitting Eq. (S1) to the temporal decays of the FAGE signal, $S_{HO2}$. The initial $HO_2$ concentration was then computed by using: $[HO_2]_0 = (S_{HO2})_0 / C_{HO2}$ to obtain values between 0.8–1.1 × $10^{11}$ molecule $cm^{-3}$.

| **$10^7$ × $C_{HO2}$[a] / counts $s^{-1}$ $mW^{-1}$ $cm^3$ $molecule^{-1}$** | **$k_{loss}$ / $s^{-1}$** |
|---|---|
| 2.00 ± 0.01 | 0.048 ± 0.001 |
| 2.13 ± 0.01 | 0.038 ± 0.001 |
| 2.34 ± 0.01 | 0.047 ± 0.001 |
| 2.30 ± 0.03 | 0.045 ± 0.002 |
| 2.07 ± 0.02 | 0.038 ± 0.002 |
| 3.01 ± 0.05 | 0.062 ± 0.002 |
| 2.50 ± 0.02 | 0.028 ± 0.001 |
| 2.78 ± 0.03 | 0.044 ± 0.002 |

[a] statistical uncertainties quoted to $1\sigma$

## S3 Kinetics of the FAGE $HO_2$ signal temporal decay at 150 mbar

The FAGE calibration factor for $HO_2$ at 150 mbar was determined by the kinetic method presented above for 1000 mbar, by fitting Eq. (S1) (Eq. (4) in the main paper) to the temporal decays of the $HO_2$ FAGE signal generated in HIRAC when the UV lamps were turned off. Nine determinations (Fig. 2 in the main text shows an example) were performed in total with the average result:

$C_{HO2} = (2.6 \pm 0.5) \times 10^{-7}$ counts cm$^3$ molecule$^{-1}$ s$^{-1}$ mW$^{-1}$,

where the error represent the overall $1\sigma$ uncertainty.

**Table S2**. FAGE calibration factor for $HO_2$, $C_{HO2}$, and the rate coefficient of the $HO_2$ wall-loss within HIRAC, $k_{loss}$, at 150 mbar extracted by fitting Eq. (S1) to the temporal decays of the FAGE signal, $S_{HO2}$. The initial $HO_2$ concentration was then computed by using: $[HO_2]_0 = (S_{HO2})_0 / C_{HO2}$ to obtain values between 0.5–1.1 × $10^{11}$ molecule cm$^{-3}$.

| $10^7 \times C_{HO2}$[a] / counts s$^{-1}$ mW$^{-1}$ cm$^3$ molecule$^{-1}$ | $k_{loss}$ / s$^{-1}$ |
|---|---|
| 2.30 ± 0.02 | 0.079 ± 0.007 |
| 2.64 ± 0.01 | 0.099 ± 0.003 |
| 2.29 ± 0.08 | 0.088 ± 0.004 |
| 2.85 ± 0.05 | 0.093 ± 0.002 |
| 3.04 ± 0.02 | 0.103 ± 0.005 |
| 2.71 ± 0.07 | 0.084 ± 0.002 |
| 2.69 ± 0.05 | 0.083 ± 0.002 |
| 2.48 ± 0.07 | 0.088 ± 0.002 |
| 2.41 ± 0.12 | 0.051 ± 0.005 |

[a] statistical uncertainties quoted to $1\sigma$

## S4 Calibration of the distributed feedback (DFB) diode laser

The current to the DFB diode laser (NTT Electronics, NLK1S5GAAA) and the built-in thermoelectric element as well as the thermistor temperature have been controlled by a Thorlabs ITC502 driver. The laser has been calibrated using a wavemeter (Burleigh WA-1000) at the operating current of 130 mA. Figure S2 shows an example of the calibration plot.

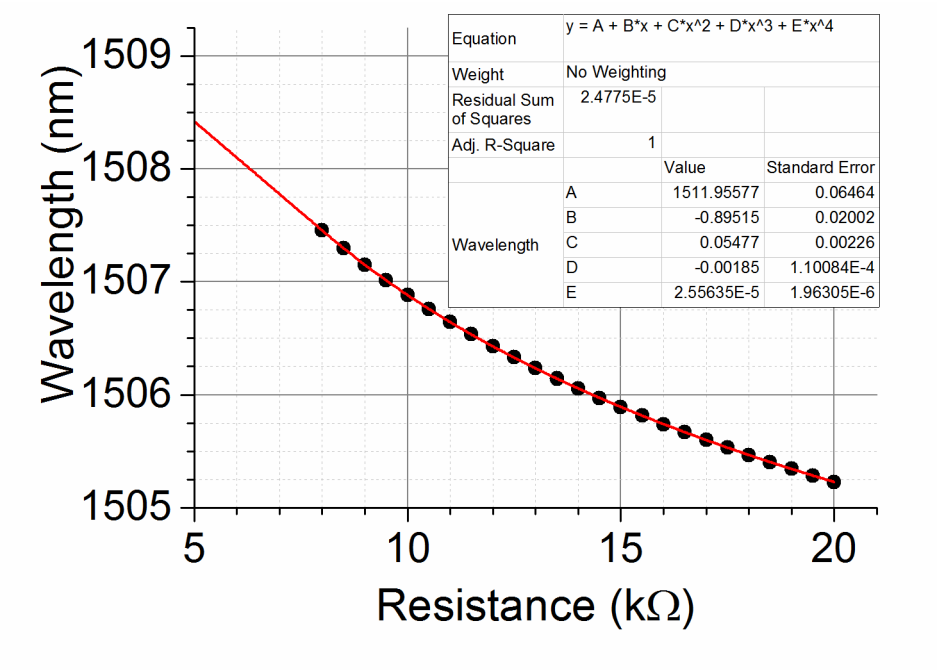


**Figure S2**. Emission wavelength vs. thermistor resistance used as calibration plot of the DFB diode laser for a current of 130 mA. The resistance of the built-in thermoelectric element is changed by varying its temperature.

During experiments the resistance is measured and the graph above used to generate the laser wavelength.

## S5 Water vapour absorption spectra

The absorption lines of water vapour nearby the region of interest for CRDS $HO_2$ measurements have been recorded to demonstrate the ability of the CRDS system to reproduce the position of the water vapour line-centres and their relative strengths as reported in the High-resolution transmission molecular absorption (HITRAN) database (Richard et al., 2012). The water vapour absorption spectrum between 1506.2 – 1506.8 nm at 150 and 1000 mbar of air have been compared to the spectra reported in HITRAN at the same pressures, and very good agreement is found, as shown Fig. S5. Almost all the five spectral features found at 150 mbar represent single absorption lines (Richard et al., 2012). At 1000 mbar the weaker spectral features, centred at 1506.66 nm and 1506.51 nm are in the noise, while the line centred at 1506.35 nm overlaps with the one at 1506.27 nm due to the pressure broadening by air.

The $H_2O$ vapour concentrations corresponding to the measurement at 150 mbar and 1000 mbar shown by the red lines in Fig. S3a and Fig. S3b, were ~ $1.5 \times 10^{15}$ molecule $cm^{-3}$ and ~ $7.5 \times 10^{14}$

molecule $cm^{-3}$, respectively, and were achieved by injecting $H_2O$ in the liquid phase into a stream of $N_2$ which was then delivered to HIRAC, which had previously been filled with synthetic air. The delivered [$H_2O_{vapour}$] was determined from FTIR measurements (Sect. S8) performed a few minutes after the $H_2O$ delivery to allow for the mixing within the chamber. At both pressures under typical HIRAC background conditions, i.e. without adding water to the chamber, $H_2O$ vapour was present at concentrations of $10^{13}$–$10^{14}$ molecule $cm^{-3}$.

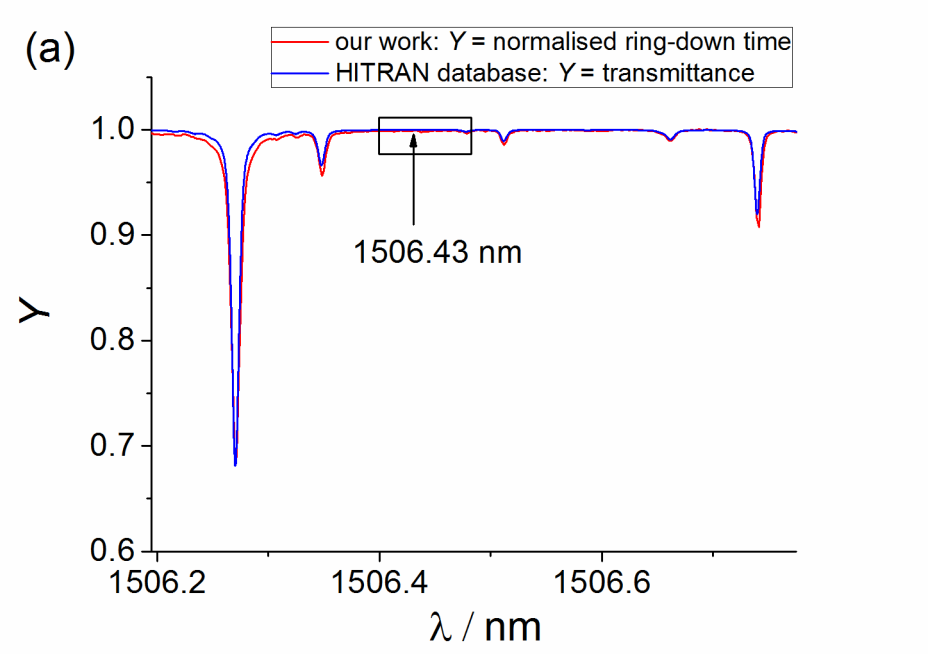

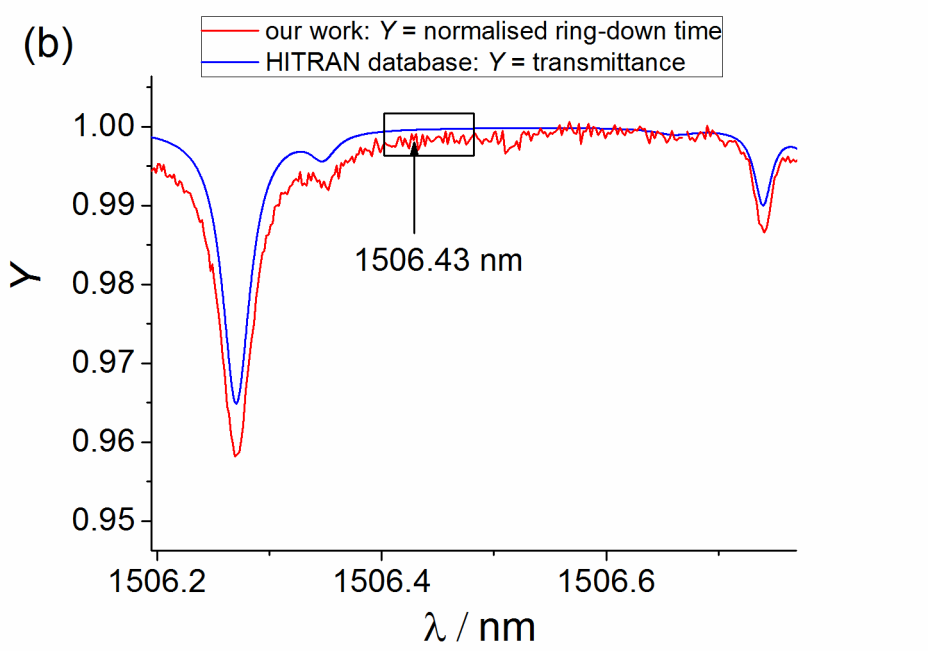


**Figure S3**. Water vapour spectrum at (a) 150 mbar and (b) 1000 mbar total pressure of synthetic air recorded inside HIRAC. The experimental concentration of $H_2O$ is ~ 1.5 × $10^{15}$ molecule $cm^{-3}$ (150 mbar) and ~ 7.5 × $10^{14}$ molecule $cm^{-3}$ (1000 mbar), calibrated using FTIR spectroscopy inside HIRAC. The red line represents the recorded ring-down time ($\tau$) divided by $\tau_{1506.6\ nm}$ and the blue line is the transmission spectrum of $H_2O$ computed using HITRAN (Richard et al., 2012) for the experimental [$H_2O$] at each operating pressure. The arrow is pointing to the value of 1506.43 nm, which was used in all the fixed wavelength measurements for $HO_2$ detection, while the black rectangle shows the wavelength range scanned to find the spectral features of $HO_2$ shown in the experimental section in the main paper (Fig. 3).

## S6 Comparison of the CRDS measurements with the HIRAC fans on to the measurements with the fans off

The ring-down time was recorded continuously in the absence of $HO_2$ under constant conditions ($T$ = 295 K, $p$ = 1000 mbar of synthetic air) and maintaining the HIRAC fans on and off, respectively, for a period of ~ 1.2 hours, as shown in Fig. S4a. The generated Allan deviation plots (Fig. S4b) show that for a signal-to-noise ratio ($S/N$) of 2, the minimum detectible absorption coefficient corresponding to a single ring-down measurement is $\alpha_0$ = 7.2 × $10^{-10}$ $cm^{-1}$ if the fans are on, which reduces to $\alpha_0$ = 4.8 × $10^{-10}$ $cm^{-1}$ if the fans are off. For $S/N$ = 2, the best CRDS sensitivity is achieved by averaging ~ 600 ring-down events (requiring 60 s at an acquisition rate of 10 Hz) and giving a minimum absorption coefficient of $\alpha_0$ = 5.4 × $10^{-11}$ $cm^{-1}$ when the fans are on and $\alpha_0$ = 4.0 × $10^{-11}$ $cm^{-1}$ when the fans are not in use.

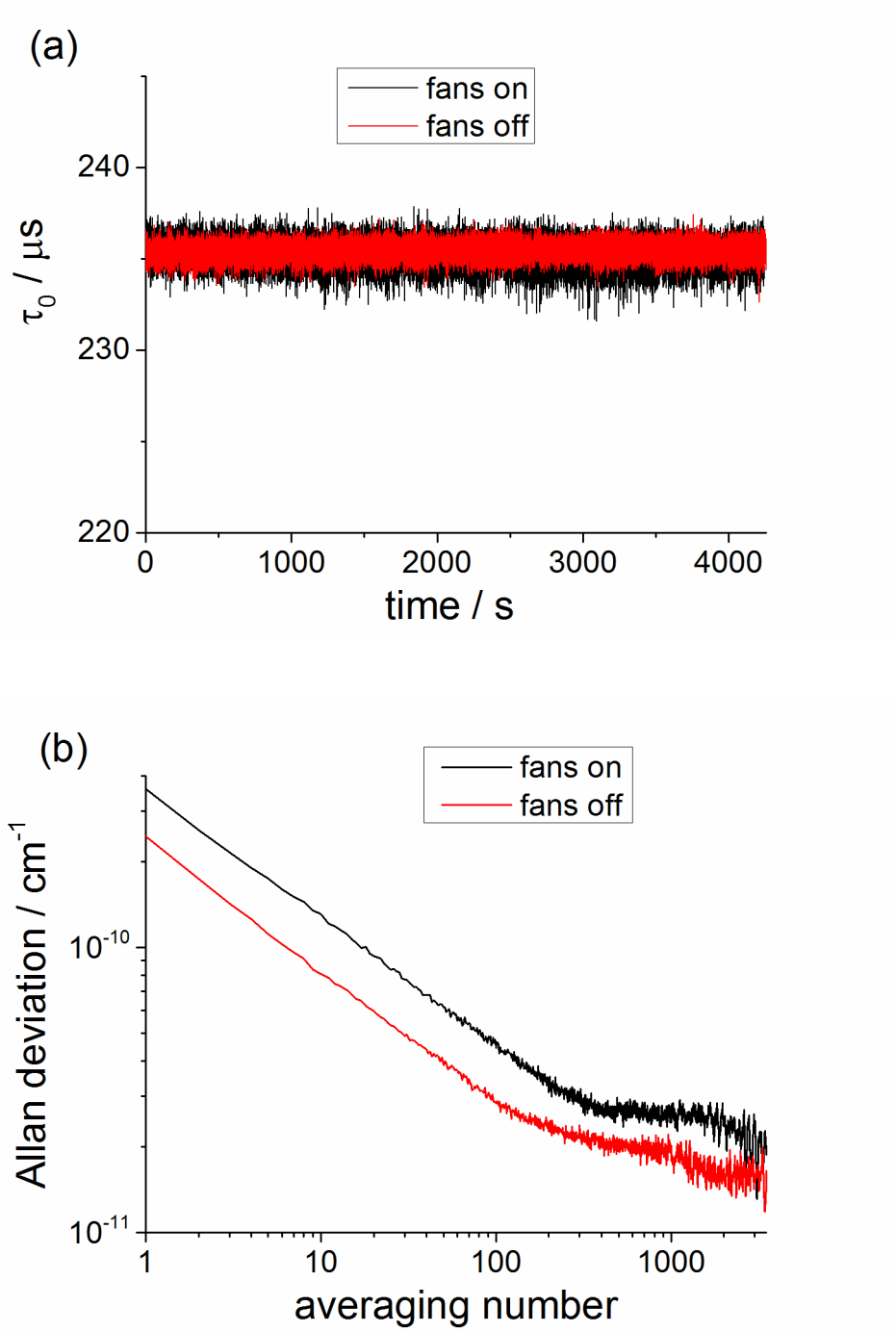


**Figure S4**. (a) Measurement of the single ring-down events at 1000 mbar of air maintaining the chamber fans on (black line) and off (red line) during ~ 1.2 hours of measurements, and (b) the corresponding Allan deviation plots of the absorption coefficient at 1506.43 nm vs. the number of ring-down events averaged.

**S7 Determination of $\sigma_{CH3OH}$ in the ~ 1506.4–1506.5 nm wavelength range.**

The absorption cross-section of $CH_3OH$ at 1506.43 nm, $\sigma_{CH3OH}$, has been determined at both HIRAC operating pressures (150 mbar and 1000 mbar) by measuring the ring-down time at 1506.43 nm, $\tau$, before and after delivering known concentrations of $CH_3OH$ to the chamber. The absorption coefficient at 1506.43 nm, $\alpha$, was computed using Eq. (S2).

$$\alpha = \frac{1}{c}\left(\frac{1}{\tau} - \frac{1}{\tau_0}\right), \qquad \text{(S2)}$$

Here $\tau_0$ is the ring-down time before adding $CH_3OH$ to HIRAC, which has been filled with synthetic air at 150 mbar and 1000 mbar, respectively. As $\sigma_{CH3OH} = \frac{\alpha}{[CH3OH]}$, $\sigma_{CH3OH}$ was obtained as the gradient of the linear fit of $\alpha$ vs. $[CH_3OH]$ (Fig. S5) where the intercept was fixed to zero. Figure S6 shows laser wavelength scans at the two chamber pressures, $\tau$ vs. $\lambda$, performed over the wavelength range of interest, ~1506.39–1506.48 nm, after delivering $CH_3OH$ in typical concentrations. The $CH_3OH$ addition produced a decrease in the ring-down time: $(\Delta\tau/\tau_0)_{150\ mbar} \cong 0.05$ and $(\Delta\tau/\tau_0)_{1000\ mbar} \cong 0.10$. At both pressures the $CH_3OH$ absorption is practically constant across all the scanned wavelength range.

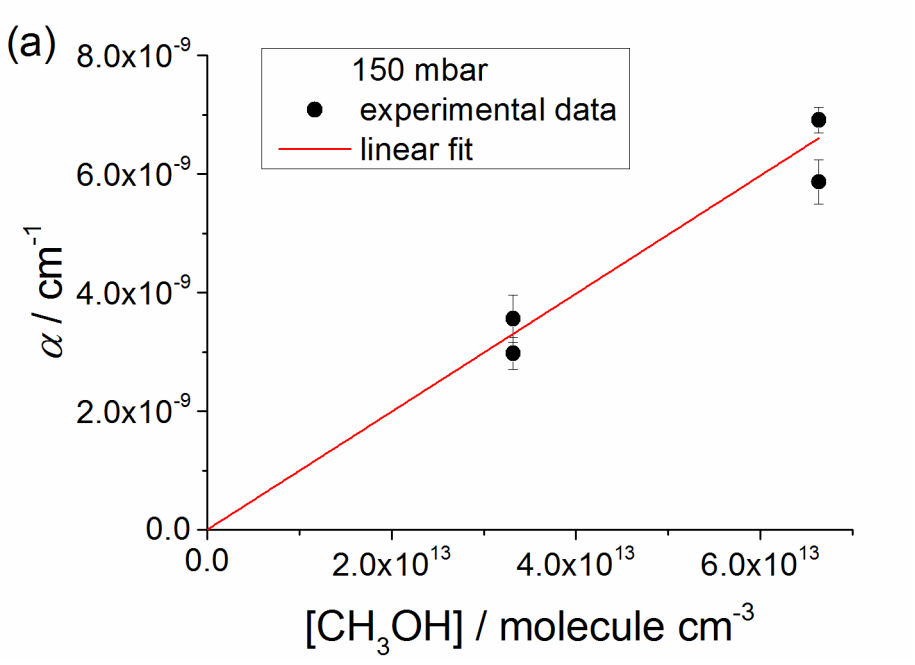

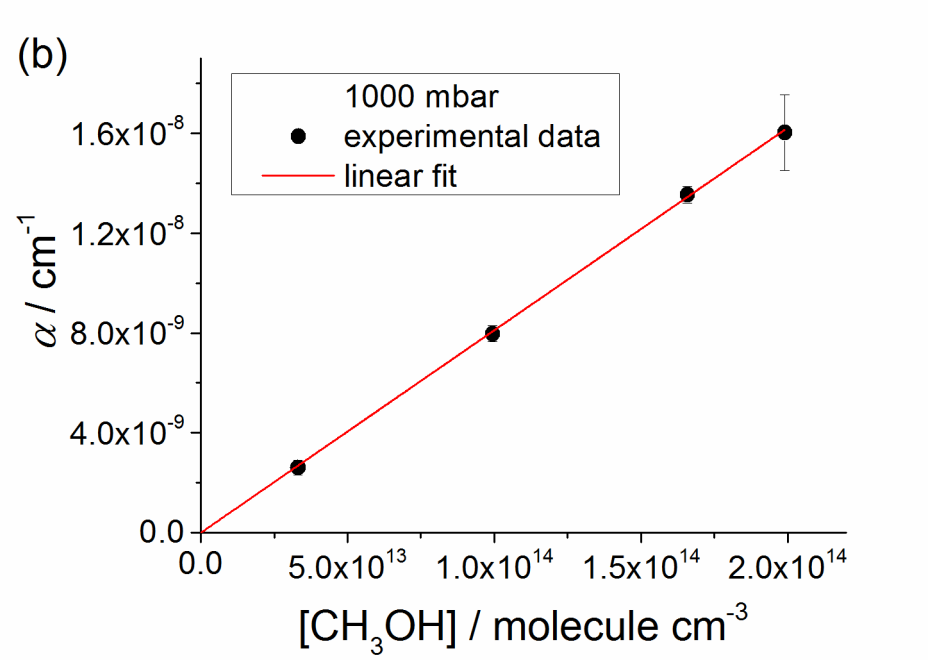


**Figure S5**. Absorption coefficient at 1506.43 nm, $\alpha$, as a function of $CH_3OH$ concentration at (a) 150 mbar and (b) 1000 mbar.. The gradient of the linear fit (red line) represents the $CH_3OH$ cross section at 1506.43 nm: $\sigma_{CH3OH,\ 150\ mbar}$ = (9.95 ± 0.42) × $10^{-23}$ $cm^2$ molecule and $\sigma_{CH3OH,\ 1000\ mbar}$ = (8.11 ± 0.05) × $10^{-23}$ $cm^2$ $molecule^{-1}$ (statistical error at 1sigma level).

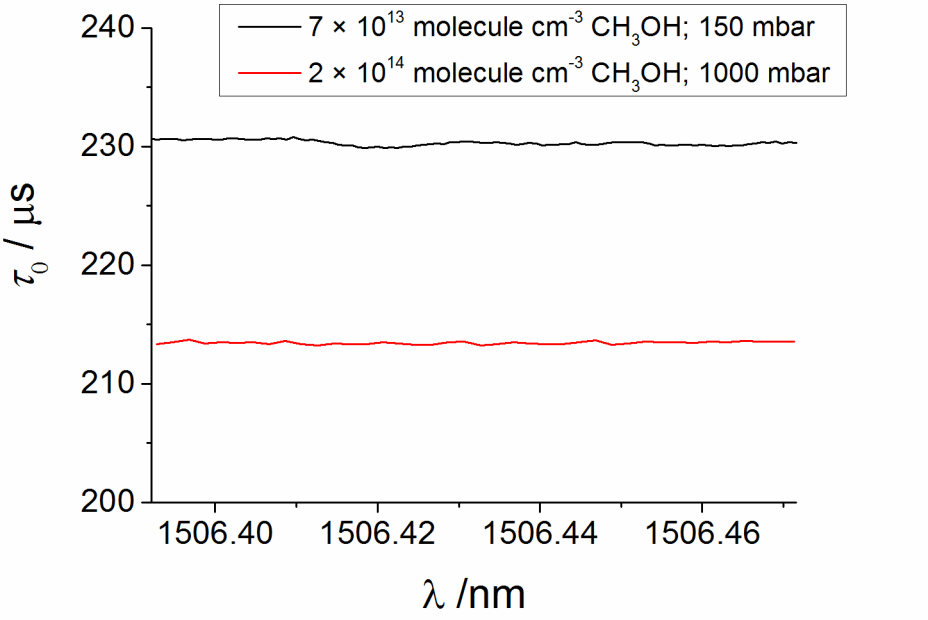


**Figure S6**. Ring down-time, $\tau$, after delivering $CH_3OH$ to HIRAC as a function of wavelength in the range of the scanned $HO_2$ absorption feature (Fig. 3 in the main manuscript) at the two applied pressures: $[CH_3OH]_0$ = 7 × $10^{13}$ molecule $cm^{-3}$; 150 mbar (black line) and $[CH_3OH]_0$ = 2 × $10^{14}$ molecule $cm^{-3}$; 1000 mbar (red line).

**S8 FTIR measurements**

$CH_3OH$ was detected during the experiments using *in situ* multi-pass FTIR along the long axis of HIRAC. The multi-pass Chernin arrangement within the chamber was optimised for 72 internal reflections giving an approximate total path length of 128.5 m (Glowacki et al., 2007;Winiberg et al., 2016). IR spectra were recorded every half a minute as the average of 30 scans (30 s integration time) at 1 $cm^{-1}$ resolution. [$CH_3OH$] during the experiments was obtained using the absorption at ~ 1030 $cm^{-1}$ due to the C-O stretch by using reference spectra at 150 and 1000 mbar taken of methanol delivered in known concentrations to the chamber. Two methods of delivery were used: (i) injecting a known volume of liquid $CH_3OH$ in a $N_2$ stream delivered to HIRAC and (ii) delivering $CH_3OH$ vapour at a known pressure to a one litre stainless steel cylinder followed by the delivery of the $CH_3OH$ from the cylinder to the chamber using a flow of $N_2$. A virtually identical $CH_3OH$ absorption spectrum in the range 700–4000 $cm^{-1}$ was measured when the same amount of $CH_3OH$ was delivered to HIRAC using separately the two methods.

**S9 Determination of $\sigma_{HO2}$(1506.43 nm)**

**S9.1 $\sigma_{HO2}$(1506.43 nm) vs. pressure between 0–1100 mbar of air**

The cross section of $HO_2$ at 1506.43 nm in the range 0–1100 mbar of air was computed by using a model which takes into account the line centred at 1506.43 nm together with the contribution of the neighbouring transitions, due to the air-broadening of the absorption lines (details in Sect. 3.2 in the main text). The simplest equation that fits well the obtained data, $\sigma_{HO2}$ as a function of pressure, was:

$$\sigma_{HO2} = A_0 + A_1\exp(-\lambda_1 p) + A_2\exp(-\lambda_2 p). \quad \text{(S3)}$$

The values of the fit parameters, $A_0$, $A_1$, $A_2$, $\lambda_1$ and $\lambda_2$ are given in Table S3.

**Table 3**. Parameters generated by fitting Eq. (S3) to $\sigma_{HO2}$(1506.43 nm) vs. pressure (in mbar) computed by application of pressure broadening to the spectral lines reported by Thiebaud et al. (2017).

| $\sigma_{HO2} = A_0 + A_1\exp(-\lambda_1 p) + A_2\exp(-\lambda_2 p)$ | | |
|---|---|---|
| $A_0$ | $(2.88 \pm 0.04) \times 10^{-20}$ | cm$^2$ molecule$^{-1}$ |
| $A_1$ | $(2.91 \pm 0.04) \times 10^{-19}$ | cm$^2$ molecule$^{-1}$ |
| $\lambda_1$ | $(1.36 \pm 0.04) \times 10^{-2}$ | mbar$^{-1}$ |
| $A_2$ | $(8.87 \pm 0.34) \times 10^{-20}$ | cm$^2$ molecule$^{-1}$ |
| $\lambda_2$ | $(2.76 \pm 0.1) \times 10^{-3}$ | mbar$^{-1}$ |

### S9.2 $\sigma_{HO2}$(1506.43 nm) at 150 mbar using the kinetics of the $HO_2$ temporal decay

The kinetics of the temporal decay monitored by CRDS when HIRAC UV lamps were turned off, i.e. $HO_2$ absorption coefficient at 1506.43 nm ($\alpha_{HO2}$) vs. time, has been used to determine $\sigma_{HO2}$ at 150 mbar. $\sigma_{HO2}$ was obtained by fitting Eq. (S4) (Eq. (10) in the main paper) to the experimental temporal decays of $\alpha_{HO2}$.

$$(\alpha_{HO_2})_t = \left( \left( \frac{1}{(\alpha_{HO_2})_0} + \frac{2 \cdot k_{\text{self-r.}}}{k_{\text{loss}} \cdot \sigma_{HO_2}} \right) \times \exp(k_{\text{loss}} t) - \left( \frac{2 \cdot k_{\text{self-r.}}}{k_{\text{loss}} \cdot \sigma_{HO_2}} \right) \right)^{-1}, \quad \text{(S4)}$$

where $(\alpha_{HO2})_t$ and $(\alpha_{HO2})_0$ are the absorption coefficient at time $t$ and $t = 0$ (the time when the UV lamps were extinguished), $k_{\text{self-r.}} = 1.79 \times 10^{-12}$ cm$^{-3}$ molecule$^{-1}$ s$^{-1}$ is the overall $HO_2$ self-reaction rate coefficient, i.e. the sum of the bimolecular rate coefficient of Reaction (R1) and the termolecular rate coefficient of Reaction (R2) at 150 mbar of air, and $k_{\text{loss}}$ is the rate coefficient describing the $HO_2$ wall-loss (Reaction (R3)).

A total of eight independent determinations were performed with the results presented in Table S4; the average results are: $\sigma_{HO2} = (1.02 \pm 0.03) \times 10^{-19}$ cm$^2$ molecule$^{-1}$ and $k_{\text{loss}} = (0.11 \pm 0.01)$ s$^{-1}$ (the error limits represent statistical errors at $1\sigma$ level).

**Table S4**. $\sigma_{HO2}$(1506.43 nm) and the rate coefficient of the $HO_2$ wall-loss within HIRAC, $k_{loss}$, at 150 mbar extracted by fitting Eq. (S4) to the experimentally recorded $\alpha_{HO2}$ vs. time.

| $10^{19} \times \sigma_{HO2}$[a] / cm$^2$ molecule$^{-1}$ | $k_{loss}$ / s$^{-1}$ |
|---|---|
| 1.02 ± 0.03[b] | 0.109 ± 0.004 |
| 0.98 ± 0.01[b] | 0.105 ± 0.003 |
| 1.01 ± 0.01[b] | 0.110 ± 0.003 |
| 1.01 ± 0.02[b] | 0.105 ± 0.004 |
| 1.02 ± 0.01[b] | 0.108 ± 0.003 |
| 1.06 ± 0.04[c] | 0.120 ± 0.006 |
| 1.02 ± 0.05[c] | 0.110 ± 0.005 |
| 1.07 ± 0.07[c] | 0.109 ± 0.006 |

[a] uncertainties quoted to $1\sigma$
[b] $[HO_2]_0$ = (1.03 ± 0.04) × $10^{11}$ molecule cm$^{-3}$ (obtained by using: $[HO_2]_0 = (\alpha_{HO2})_0 / \sigma_{HO2}$)
[c] $[HO_2]_0$ = (4.72 ± 0.04) × $10^{10}$ molecule cm$^{-3}$ (computed by using: $[HO_2]_0 = (\alpha_{HO2})_0 / \sigma_{HO2}$)

### S9.3 $\sigma_{HO2}$ (1506.43 nm) at 1000 mbar using the kinetics of the $HO_2$ temporal decay

In order to improve the precision of the $\sigma_{HO2}$ determination at 1000 mbar, the FAGE signal decays recorded at the same time with the $\alpha_{HO2}$ decays were used to determine $\sigma_{HO2}$. The fluorescence signal decays were scaled to overlap $\alpha_{HO2}$ vs. time by multiplying the FAGE signal with $f = \frac{(\bar{\alpha}_{HO_2})_0}{(\bar{S}_{HO_2})_0}$, where $(\bar{\alpha}_{HO_2})_0$ and $(\bar{S}_{HO_2})_0$ are the average absorption coefficient and the mean FAGE signal before the UV lamps are switched off. Equation (S4), where the overall $HO_2$ self-reaction rate coefficient $k_{self\text{-}r.}$ was fixed to 2.85 × $10^{-12}$ cm$^{-3}$ molecule$^{-1}$ s$^{-1}$ (Atkinson et al., 2004), was fitted to the scaled signal decays to obtain $\sigma_{HO2}$ and $k_{loss}$. Six determinations were carried out in total with the results shown in Table S5; the average results are: $\sigma_{HO2}$ = (3.87 ± 0.12) × $10^{-20}$ cm$^2$ molecule$^{-1}$ and $k_{loss}$ = (0.045 ± 0.004) s$^{-1}$ (the error limits represent statistical errors at $1\sigma$ level).

**Table S5**. $\sigma_{HO2}$(1506.43 nm) and the wall-loss rate coefficient within HIRAC, $k_{loss}$, at 1000 mbar obtained by fitting Eq. (S4) to the temporal decays obtained by multiplying the FAGE signal, $\left(S_{HO_2}\right)_t$, with $f = \frac{\left(\bar{\alpha}_{HO_2}\right)_0}{\left(\bar{S}_{HO_2}\right)_0}$, where $\left(\bar{\alpha}_{HO_2}\right)_0$ and $\left(\bar{S}_{HO_2}\right)_0$ are the average absorption coefficient and the mean FAGE signal before the UV lamps are extinguished.

| $10^{20} \times \sigma_{HO2}$[a] / cm$^2$ molecule$^{-1}$ | $k_{loss}$ / s$^{-1}$ |
|---|---|
| 3.65 ± 0.04[b] | 0.046 ± 0.004 |
| 3.54 ± 0.06[b] | 0.029 ± 0.008 |
| 3.29 ± 0.05[b] | 0.028 ± 0.002 |
| 4.08 ± 0.06[b] | 0.034 ± 0.005 |
| 4.30 ± 0.30[c] | 0.070 ± 0.011 |
| 4.36 ± 0.13[c] | 0.062 ± 0.004 |

[a] uncertainties quoted to $1\sigma$
[b] $[HO_2]_0$ = (9.94 ± 0.25) × $10^{10}$ molecule cm$^{-3}$ (obtained by using: $[HO_2]_0 = (\alpha_{HO2})_0 / \sigma_{HO2}$)
[c] $[HO_2]_0$ = (5.96 ± 0.11) × $10^{10}$ molecule cm$^{-3}$ (computed by using: $[HO_2]_0 = (\alpha_{HO2})_0 / \sigma_{HO2}$)

## S10 Intercomparison of CRDS and FAGE $HO_2$ measurements

In some intercomparison experiments the lamps were alternately turned on for 2–3 min and then off for ~ 3 min to generate a series of typically three $HO_2$ temporal decays followed by regeneration of the $HO_2$ (Figs. S9 and S10).

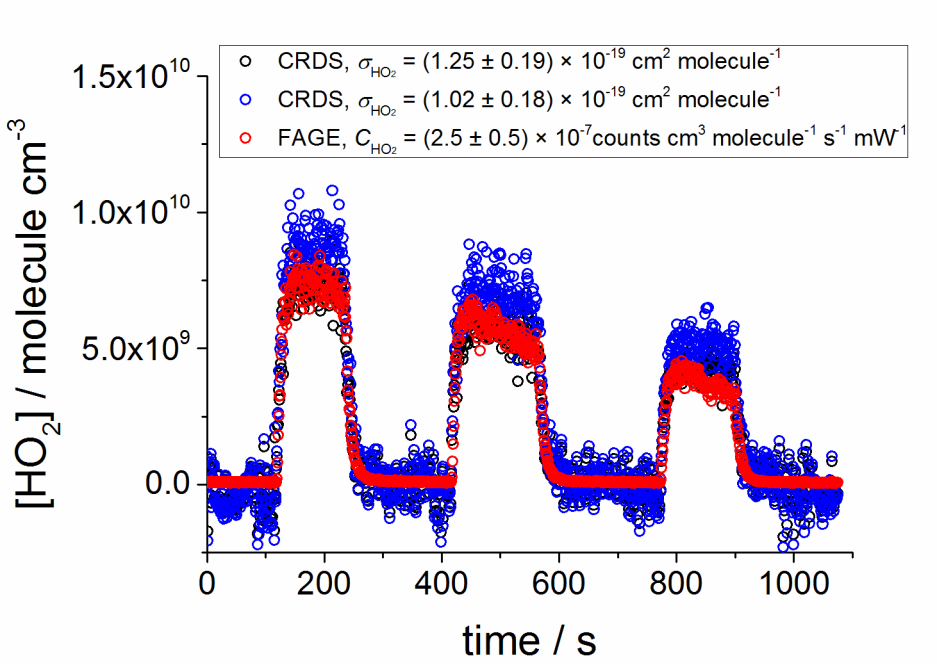


**Figure S7**. Comparison measurement at 150 mbar where the lamps were alternatively turned on and then off, every time for 100–200 s. [$HO_2$] was computed using a FAGE calibration factor $C_{HO2}$ = 2.6 × 10$^{-7}$ counts cm$^3$ molecule$^{-1}$ s$^{-1}$ mW$^{-1}$ (red) and a cross section at 1506.43 nm $\sigma$ = 1.25 × 10$^{-19}$ cm$^2$ molecule$^{-1}$ (black) and $\sigma$ = 1.02 × 10$^{-19}$ cm$^2$ molecule$^{-1}$ (blue) - details in the main paper. Data averaged over 1 sec. Concentrations at time zero: [$CH_3OH$]$_0$ = 6.6 × 10$^{13}$ molecule cm$^{-3}$, [$Cl_2$]$_0$ = 7.1 × 10$^{12}$ molecule cm$^{-3}$.

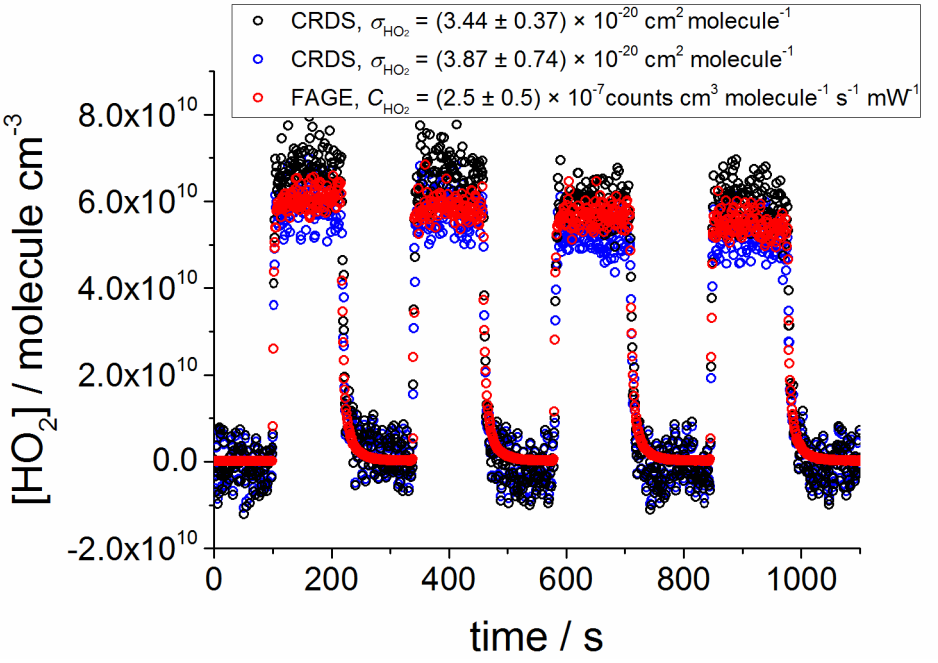


**Figure S8**. Comparison measurement at 1000 mbar where the lamps were alternatively turned on and then off, every time for 100–200 s. [$HO_2$] was computed using the FAGE calibration factor obtained by averaging the values determined by the two calibration methods, the $H_2O$ photolysis and the kinetics of the $HO_2$ decays, $C_{1000\ mbar}$ = 2.5 × 10$^{-7}$ counts cm$^3$ molecule$^{-1}$ s$^{-1}$ mW$^{-1}$ (red) and a cross section at 1506.43 nm $\sigma$ = 3.44 × 10$^{-20}$ cm$^2$ molecule$^{-1}$ (black) and $\sigma$ = 3.87 × 10$^{-20}$ cm$^2$ molecule$^{-1}$ (blue) ) - details in the main paper. Data averaged over 1 sec. Concentrations at time zero: [$CH_3OH$]$_0$ ~ 8 × 10$^{13}$ molecule cm$^{-3}$, [$Cl_2$]$_0$ ~ 4 × 10$^{13}$ molecule cm$^{-3}$.

## References

Atkinson, R., Baulch, D. L., Cox, R. A., Crowley, J. N., Hampson, R. F., Hynes, R. G., Jenkin, M. E., Rossi, M. J., and Troe, J.: Evaluated kinetic and photochemical data for atmospheric chemistry: Volume I - gas phase reactions of Ox, HOx, NOx and SOx species, Atmospheric Chemistry and Physics, 4, 1461-1738, 2004.

Glowacki, D. R., Goddard, A., Hemavibool, K., Malkin, T. L., Commane, R., Anderson, F., Bloss, W. J., Heard, D. E., Ingham, T., Pilling, M. J., and Seakins, P. W.: Design of and initial results from a Highly Instrumented Reactor for Atmospheric Chemistry (HIRAC), Atmos. Chem. Phys., 7, 5371-5390, 2007.

Richard, C., Gordon, I. E., Rothman, L. S., Abel, M., Frommhold, L., Gustafsson, M., Hartmann, J. M., Hermans, C., Lafferty, W. J., Orton, G. S., Smith, K. M., and Tran, H.: New section of the HITRAN database: Collision-induced absorption (CIA), J. Quant. Spectrosc. Ra., 113, 1276-1285, 10.1016/j.jqsrt.2011.11.004, 2012.

Winiberg, F. A. F., Dillon, T. J., Orr, S. C., Gross, C. B. M., Bejan, I., Brumby, C. A., Evans, M. J., Smith, S. C., Heard, D. E., and Seakins, P. W.: Direct measurements of OH and other product yields from the $HO_2$ +$CH_3C(O)O_2$ reaction, Atmos. Chem. Phys., 16, 4023-4042, 2016.